Key Points:
- We test if the presence of pseudotachylytes in the Gole Larghe fault is consistent with predictions from thermal pressurization
- Thermal pressurization is too efficient to explain melting, except if "damaged" rock properties are considered

Supporting Information:
- Supporting Information S1

Correspondence to:
N. Brantut,
n.brantut@ucl.ac.uk

Assessing the Efficiency of Thermal Pressurization Using Natural Pseudotachylyte-Bearing Rocks

Nicolas Brantut[1] [ID] **and Thomas M. Mitchell[1]** [ID]

[1]Department of Earth Sciences, University College London, London, UK

Abstract The efficiency of thermal pressurization as a dynamic weakening mechanism relies on the thermal and hydraulic properties of the rocks forming the fault core. Here we assess the effectiveness of thermal pressurization by comparing predictions of temperature rise to field estimates based on pseudotachylyte-bearing rocks. We measure hydraulic and transport properties of a suite of fault rocks (a healed cataclasite, an unhealed breccia, and the intact parent rock) from the pseudotachylyte-bearing Gole Larghe fault in the Adamello batholith (Italy) and use them as inputs in numerical simulations of thermal pressurization. We find that the melting temperature can be reached only if damaged, unhealed rock properties are used. A tenfold increase in permeability or a fourfold increase in pore compressibility of the intact rock is required to achieve melting. Our results emphasize the importance of damage processes that strongly modify fault rock properties and dynamic weakening processes during earthquake propagation.

Plain Language Summary During earthquakes, faults slide rapidly past each other, typically at several meters per second. Such fast sliding rates at great depth in the crust are expected to generate large amounts of heat and should melt the rocks at the sliding interface. However, such melted rocks are not systematically observed in faults. A number of mechanisms have been suggested to explain this apparent discrepancy. One convincing explanation is that the presence of water within the porosity of the fault rocks buffers the fault temperature by being rapidly pressurized and reducing the fault friction. This effect has been predicted from physical models, but these predictions depend strongly on poorly constrained rock properties and have not yet been tested in nature. Here we measured key physical properties in rocks adjacent to a fault that underwent frictional melting, and we test whether model predictions for the effects of pressurized water are consistent with the presence of melt. We find that it is the case only if rock properties are altered to account for the effect of microfractures that are likely created during earthquake rupture. Our results provide constrains to improve earthquake simulations and highlight the key role of microfracture damage on fault sliding processes.

1. Introduction

Weakening of faults during seismic slip is generally considered to be driven by power dissipation and shear heating (Di Toro et al., 2011). In fluid-saturated fault rocks, shear heating is likely to induce weakening by locally increasing the pore fluid pressure, a process called *thermal pressurization* (Lachenbruch, 1980; Mase & Smith, 1985; Rice, 2006; Sibson, 1975). In addition to triggering substantial weakening, thermal pressurization also maintains faults under relatively low temperature and can prevent frictional melting (e.g., Acosta et al., 2018; Rempel & Rice, 2006).

Frictional melting during seismic slip is recognized in exhumed fault zones as pseudotachylytes, which are frozen melt layers containing originally glassy material. Pseudotachylytes are widely recognized as an unequivocal geological record of seismogenic slip along ancient active faults. As they originate from coseismic shear heating, their presence and characteristics also provide key constraints on the shear stresses and power dissipation rates acting during the earthquakes that led to their formation (e.g., Di Toro et al., 2005). The very existence of pseudotachylytes also implies that other weakening mechanisms and thermal buffering processes, such as thermal or chemical (due to devolatilization reactions) pressurization, were not efficient enough to prevent melting.

In fluid-saturated rocks the efficiency of thermal pressurization as a weakening mechanism (i.e., how quickly and how much strength is reduced from the initial static strength) and as a thermal buffer (limiting how high

the temperature can rise during sliding) is governed by a number of physical properties of the fault rock hosting the slip event: thermal capacity, heat diffusivity, poroelastic storage capacity, hydraulic diffusivity, thermal expansivity of the pore space, and slip-induced dilation/compaction factors. The effect of thermal pressurization is typically predicted based on parameter values measured in the laboratory. For instance, Noda and Shimamoto (2005) and Wibberley and Shimamoto (2005) measured permeability, porosity, and compressibility on fault gouges sampled along major active faults to predict the slip-weakening behavior of those faults during earthquakes. Similarly, Rice (2006; followed by a large number of subsequent studies) used physical parameters measured in a natural fault gouge (determined by Wibberley & Shimamoto, 2003) to make general predictions of the characteristic slip weakening distance for upper crustal earthquakes.

One major challenge when using laboratory-derived data to compute the effects of thermal pressurization is that the laboratory measurements are conducted on exhumed or subsurface rocks under static conditions that are not representative of the natural conditions prevailing during earthquake slip. In particular, the strong dynamic changes in stress occurring during earthquake propagation are expected to produce significant off-fault damage and therefore strongly increase the permeability of the host rocks (e.g., Mitchell & Faulkner, 2012). Some ad hoc procedures have been suggested by Rice (2006; and subsequently used by Rempel & Rice, 2006, and Noda et al., 2009) to account for damage in a phenomenological way, by artificially increasing the hydraulic diffusivity of the fault rocks by an arbitrary factor. Despite these efforts, a true assessment of the effect of damage and of the efficiency of thermal pressurization remains to be achieved.

Here we use pseudotachylyte-bearing rocks as a natural thermometer to test predictions from thermal pressurization, assuming that the rocks are initially fluid-saturated and using laboratory-derived rock properties as model input. We sampled a range of rocks from the Gole Larghe Fault zone (GLFZ), Italy (Di Toro et al., 2004; Smith et al., 2013), and measured their transport properties as a function of confining pressure in the laboratory. We then use these data in a thermal pressurization model to predict the peak temperature achieved during a seismic event with comparable magnitude to that which generated the field pseudotachylytes. We test whether these predictions are compatible with the occurrence of pseudotachylytes, and what are the key parameters and unknowns controlling the onset of melting. Overall, we show that using laboratory data from near-fault rocks directly into thermal pressurization simulations is not compatible with frictional melting and that some effect of damage (e.g., an increase in storage capacity or permeability) must be accounted for to explain the field observations. Our conclusions highlight the key importance of damage generation and healing during the seismic cycle.

2. Laboratory Data on Fault Rocks From GLFZ

The GLFZ is an exhumed strike slip fault in the Adamello batholith in the Italian Southern Alps (Di Toro et al., 2004; Smith et al., 2013), crosscutting tonalite of the relatively young Val d'Avio-Val di Genova pluton (34–32 Ma; Del Moro et al., 1983). Faulting along the GLFZ occurred at around 30 Ma (Pennacchioni et al., 2006), subsequent to the pluton emplacement and concomitant with faulting along the Tonale Line (Stipp et al., 2004), at temperatures in the order of 250 to 300 °C and at a depth of 9 to 11 km. The GLFZ is a dextral strike-slip fault with a length of around 20 km and a damage zone thickness of around 500 to 600 m (Smith et al., 2013). Fault damage is characterized by faults with cataclastic cores that are primarily located on preexisting reactivated cooling joints and pseudotachylyte bearing faults. These structures strike approximately east-west and dip steeply to the south.

The presence of hydrous phases in the host cataclasites indicates that water must have been present prior to the seismic events leading to the formation of pseudotachylytes. Geochemical analyses by Mittempergher et al. (2014) suggest that the fluids were likely of metamorphic origin, but the exact pressure conditions are unknown. The chemical alteration within the cataclasites has likely closed the fault core to long term fluid flow, so that any free fluids would have remained trapped at undetermined pressures. Here we assume that free fluids, pressurized to some degree, were present immediately prior to the pseudotachylyte-forming seismic ruptures. This assumption is discussed is section 4 but is a realistic one because hydration reactions produce a net volume increase (hence their sealing capability), which has the potential to locally increase the pressure of the remaining pore fluids.

The damage structure surrounding the GLFZ at both the microscale and macroscale has been investigated previously by Smith et al. (2013) on fault perpendicular transects (Figure 1, microscale damage). Here we chose three representative samples from this study that were (a) intact, (b) damaged, and (c) healed where
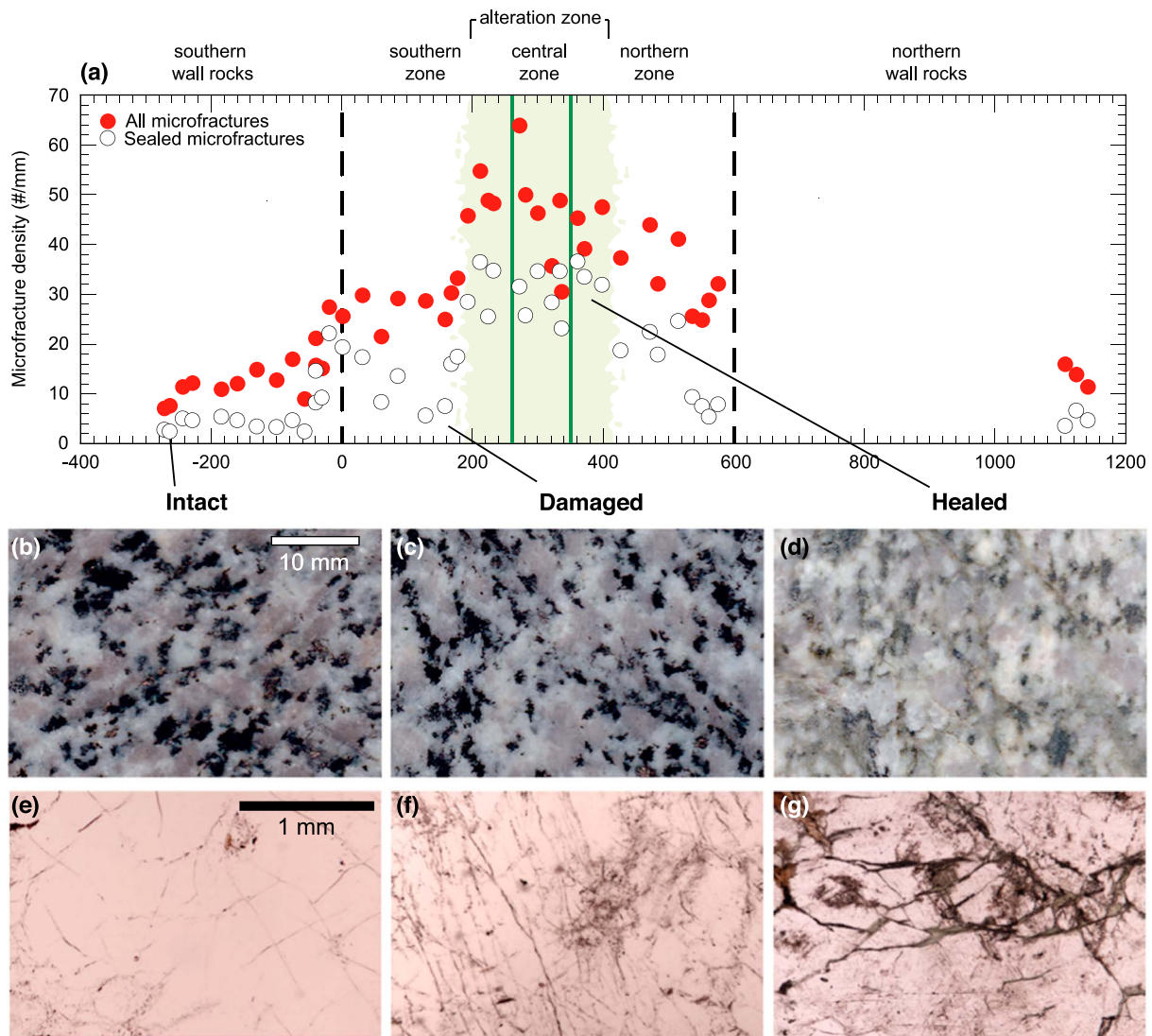
Figure 1. Microfracture density variations across the Gole Larghe Fault zone. (a) Graph of microfracture density versus distance across the fault zone. Both total microfracture density and the density of sealed microfractures are shown (modified from Smith et al., 2013). (b–d) Images of scanned cut surfaces of the intact, damaged, and sealed samples. Macroscopically, both the intact and damaged samples are similar, indicating the majority of damage is microscopic. The sealed sample illustrates the progressive transformation of brown biotite in the host rock to green chlorite approaching the central area of the Gole Larghe Fault zone. (e–g) Optical images of thin sections of intact, damaged, and sealed samples, including traces of microfracture damage.

microfracture damage was previously quantified, and prepared additional samples from the same blocks for measurements of permeability.

Microfracture densities are low in the host rock outside the damage zone at −300 m, and this is our sample (a) "intact." From the edge of the fault zone, microfracture density increases with increasing proximity to the fault core. We select a representative sample at around −210 m of (b) "damaged" rock, where open microfracture density is highest. While microfracture density is highest between 2-m-thick cataclastic bands that define the central core zone, microfractures are frequently sealed with K-feldspar, epidote and chlorite, also recognizable in the field by the green coloring of the rocks (Figure 1c), and this represents our (c) "healed" sample.

We prepared samples from the same oriented blocks collected by Smith et al. (2013). Cylindrical cores with lengths and diameter of up to 75 and 30 mm, respectively, were prepared, with the core axis perpendicular to the GLFZ plane. The experimental setup consisted of a pressure vessel in which a jacketed sample was subjected to hydrostatic pressure using oil as the confining medium. The pore pressure system, comprising an
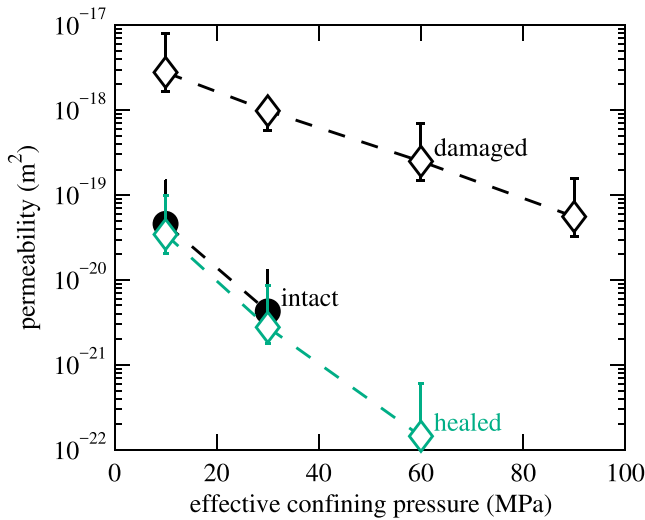
Figure 2. Permeability as a function of effective pressure for three representative samples of the intact, damaged-healed, and damaged tonalite hosting the pseudotachylytes.

upstream and a downstream reservoir, was filled with distilled water. Confining pressure and upstream pore pressure were hydraulically servo controlled (e.g., Duda & Renner, 2013).

The permeability of rock samples was measured as a function of effective confining pressure using the method of pore pressure oscillation (Bernabé et al., 2006; Fischer & Paterson, 1992). The results are shown in Figure 2. The permeability of the damaged-healed tonalite is the same as that of the intact one (sampled far from the fault zone) and decreases from around 4×10^{-20} to 10^{-22} m^2 for effective pressures increasing from 10 to 60 MPa. The damaged tonalite is significantly more permeable than the intact one, with a permeability ranging from 3×10^{-18} m^2 at 10 MPa effective pressure down to 6×10^{-20} m^2 at 90 MPa effective pressure. In all cases, the permeability is well approximated by a decreasing exponential:

$$k(P_{\text{eff}}) = k_0 \exp(-\kappa P_{\text{eff}}), \tag{1}$$

where P_{eff} is the effective confining pressure, k_0 is the nominal permeability value, and κ is the pressure sensitivity parameter. We find $k_0 = 9\times 10^{-20}$ m^2 and $\kappa = 1.09 \times 10^{-7}$ Pa^{-1} for the intact or damaged-healed tonalite, and $k_0 = 4 \times 10^{-18}$ m^2 and $\kappa = 4.8 \times 10^{-8}$ Pa^{-1} for the damaged tonalite.

The storage capacity of the samples could not be determined accurately across the whole pressure range by the pore pressure oscillation method employed here. However, we obtained useful upper bounds at the lowest pressures. At 10 MPa effective pressure, in the intact tonalite, a storage capacity $S \approx 9.5 \times 10^{-11}$ Pa^{-1} was estimated; in the damaged tonalite, we determined $S \approx 2.5\times 10^{-11}$ Pa^{-1}. In the damaged-healed tonalite, the storage capacity could not be determined at all: The inversion method used to extract S from the pore pressure oscillation data for this rock would only output unrealistically low values, less than the compressibility of solid (of the order of 10^{-12} Pa^{-1}).

3. Tests of Temperature Predictions From Thermal Pressurization

3.1. Governing Equations and Assumptions

During rapid shear across a narrow fault core, the temperature (T) and fluid pressure (p) increase due to shear heating and diffusion across the fault are given by (e.g., Lachenbruch, 1980)

$$\frac{\partial p}{\partial t} = \frac{1}{\rho_{\text{f}} \beta^*} \frac{\partial}{\partial y}\left(\frac{\rho_{\text{f}} k}{\eta} \frac{\partial p}{\partial y}\right) + \Lambda \frac{\partial T}{\partial t}, \tag{2}$$

$$\frac{\partial T}{\partial t} = \alpha_{\text{th}} \frac{\partial^2 T}{\partial y^2} + \frac{\tau \dot{\gamma}}{\rho c}, \tag{3}$$

where t is the time, y is the across-fault coordinate, τ is the shear stress, and $\dot{\gamma}$ is the shear strain rate. A number of material properties appear: ρ_{f} and η are the fluid density and viscosity, respectively, and β^*, k, α_{th}, and ρc are, respectively, the storage capacity, permeability, thermal diffusivity, and specific heat capacity of the fluid-saturated rock. The factor Λ is given by

$$\Lambda = \frac{\lambda_{\text{f}} - \lambda_{\text{n}}}{\beta_{\text{f}} + \beta_{\text{n}}}, \tag{4}$$

where λ_{f} and λ_{n} are the thermal expansivity coefficients of water and of the pore space, respectively, and β_{f} and β_{n} are the bulk compressibilities of water and of the pore space, respectively.

As demonstrated by Rice (2006, Appendix A), the compressibility of the pore space β_{n} is not a straightforward material parameter. Assuming elastic fault walls, it is computed as

$$\beta_{\text{n}} = \frac{(\beta_{\text{d}} - \beta_{\text{s}})(\beta_{\text{d}} + r\beta_{\text{s}})}{n(1+r)\beta_{\text{d}}} - \beta_{\text{s}}, \tag{5}$$

Table 1
List of Parameters Used in the Simulations

Parameter	Value
Normal stress, σ_n	280 MPa
Initial pore pressure, p_0	150 MPa
Initial temperature, T_0	300 °C
Shear zone width, h	10 µm
Slip rate[a], V	—
Friction coefficient, f	0.15
Porosity, n	2 %
Permeability[b], k	$k_0 e^{-\kappa \cdot P_{\text{eff}}}$
Specific heat, ρc	2.7×10^6 Pa °C^{-1}
Thermal diffusivity, α_{th}	0.7×10^{-6} m^2/s
Pore compressibility, β_n	2×10^{-9} Pa^{-1}
Pore thermal expansivity, λ_n	0 K^{-1}
Fluid density[c], ρ_f	—
Fluid compressibility[c], β_f	—
Fluid thermal expansivity[c], λ_f	—
Fluid viscosity[c], η	—

[a]Slip rate is given by a regularized Yoffe function with a maximum displacement of 0.2 m, a total duration of 1.02 s, and a smoothing time of 0.01 s. [b]Permeability is given as a function of effective pressure $P_{\text{eff}} = \sigma_n - p$ using the nominal k_0 and pressure dependency κ parameter determined in the laboratory. [c]All water properties are given as a function of pore pressure and temperature using the International Association for the Properties of Water and Steam formulation (Junglas, 2009).

where β_d is the drained compressibility of the porous rock, β_s is the compressibility of the solid skeleton, n is the porosity, and r is a function of the drained Poisson's ratio of the rock. The drained compressibility is related to the storage capacity as follows:

$$\beta_d = S - n\beta_f + (1 + n)\beta_s. \tag{6}$$

Using reasonable parameter values of $n = 0.01$, $r = 1$, $\beta_s = 2 \times 10^{-11}$ Pa^{-1} and a conservative bound for the storage capacity of $S = 3 \times 10^{-11}$ Pa^{-1} for granite (Jaeger et al., 2007), we determine an estimate of $\beta_n = 2 \times 10^{-9}$ Pa^{-1}. As a first conservative approximation, we use this value for both the intact and damaged samples and explore the impact of variations in this parameter later on.

We assume that the shear strain is homogeneous across a narrow zone of constant thickness h, so that $\dot\gamma = V/h$, where V is the slip rate during the earthquake. Thermal pressurization is known to promote strain localization, unless the shear zone thickness is very small; we therefore choose $h = 10$µm, which is equal to, or smaller than, the typical shear zone thickness obtained from spontaneous localization during thermal pressurization (Platt et al., 2014; Rice et al., 2014). This choice is a conservative one in the sense that such a narrow slip zone will tend to promote faster and higher temperature rise during slip than a wider slip zone.

We use a realistic, nonconstant slip rate history in the form of a regularized Yoffe function (Tinti et al., 2005), characterized by a maximum slip, a total duration, and a so-called "smoothing" timescale, which is a measure of the time between the onset of slip and the peak slip rate. Since pseudotachylytes are observed along small faults with offsets as small as 20 cm, we choose a maximum slip equal to 20 cm, a smoothing time of 0.01 s (so that the peak slip rate is of around 2 m/s), and a total duration of 1.02 s (i.e., typical parameters for a magnitude $M_w \sim 5$ event).

The shear stress acting on the fault during slip is assumed equal to a constant friction coefficient f multiplied by the effective normal stress $\sigma_n - p$. The friction coefficient is taken equal to 0.15, which assumes that high velocity frictional weakening (for instance due to the flash heating) has already occurred during the very early stages of slip (e.g., Brantut et al., 2016; Hayward et al., 2016).

The initial temperature of the fault is assumed to be equal to that at 10 km depth in a relatively hot continental geothermal gradient, which amounts to $T_0 = 300$ °C. In the absence of accurate constraints on the fault geometry and stress history, we follow common practice (e.g., Rice, 2006) and assume that the fault normal stress is equal to the lithostatic pressure, that is, $\sigma_n = 280$ MPa. The initial pore pressure is difficult to assess and in the absence of better constraints we choose an approximately hydrostatic fluid pressure condition of $p_0 = 100$ MPa. This hypothesis is the most common is thermal pressurization studies and is therefore an important one to test here. The effect of variations in the initial pore pressure will be tested further below.

In equations (2) and (3), all the fluid and rock properties are potentially varying (sometimes strongly) with pore pressure and temperature. Although well-chosen constant values can be used to determine typical estimates for the effect of thermal pressurization (e.g., Brantut & Platt, 2017; Rempel & Rice, 2006; Rice, 2006), here we aim to provide more accurate predictions and therefore we solve (2) and (3) including the full dependencies of parameters with pressure and temperature conditions.

The coupled system (2)–(3) is solved using a semi-implicit finite difference method (similar to that used by Brantut et al., 2010). The full list of parameter values is given in Table 1, using the laboratory-derived permeability for each rock (intact/healed, and damaged tonalite).

3.2. Results

We first performed reference computations using the parameter values as listed in Table 1. The results are shown in Figure 3. In the intact rock, the peak temperature reached during slip remains relatively low, around 770 °C, well below the bulk melting temperature of the tonalite. By contrast, in the damaged rock, the temperature rises beyond 1000 °C after only 1-cm slip, therefore predicting bulk melting early during the slip event.
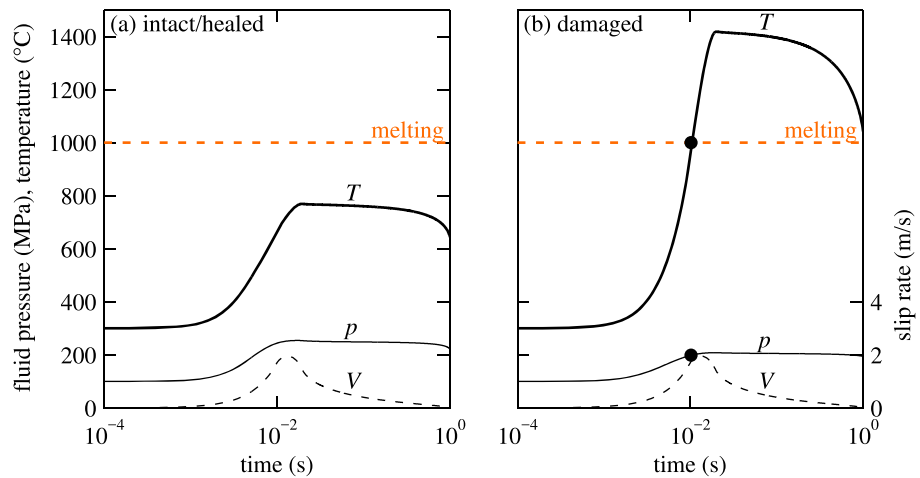
Figure 3. Reference computations of pore pressure (p) and temperature (T) with the slip rate history $V(t)$ using parameter values for (a) the intact (or damaged-healed) tonalite and (b) the damaged tonalite.

Our simulations show that the presence of pseudotachylytes is not well explained if we use our laboratory-derived values of permeability for the rock directly hosting them in the field. According to our analysis, at initially hydrostatic fluid pressure conditions in the rupture zone, pseudotachylytes should only form in the damaged tonalite. In order to investigate what level of damage is required to start forming pseudotachylyte in an intact tonalite, we computed the peak temperature achieved during slip for a range of nominal permeabilities k_0 and pore space compressibilities β_n. The compressibility of the pore space is poorly constrained, and its value is expected to be significantly affected by the occurrence of damage and microfracturing off the slip zone (Rice, 2006, Appendix A).

Figure 4 reports the results of our computations, outlining the 1000 °C isotherm as the onset of melting for each set of parameters. Starting from the intact or damaged-healed tonalite (Figure 4a), using an initial pore pressure $p_0 = 100$ MPa, we observe that a rather small increase in β_n up to around 5×10^{-9} Pa^{-1} is sufficient to explain bulk melting of the rock. By contrast, only very large increases in k_0 of around 4 orders of magnitude allow the system to reach a peak temperature above 1000 °C. Overall, simply doubling β_n to around 4×10^{-9} Pa^{-1} and increasing k_0 by 1 order of magnitude appears sufficient to explain bulk melting. A reduction in the initial pore pressure (dashed line), simulating instantaneous dilatancy at the onset of slip (Rice, 2006), tends
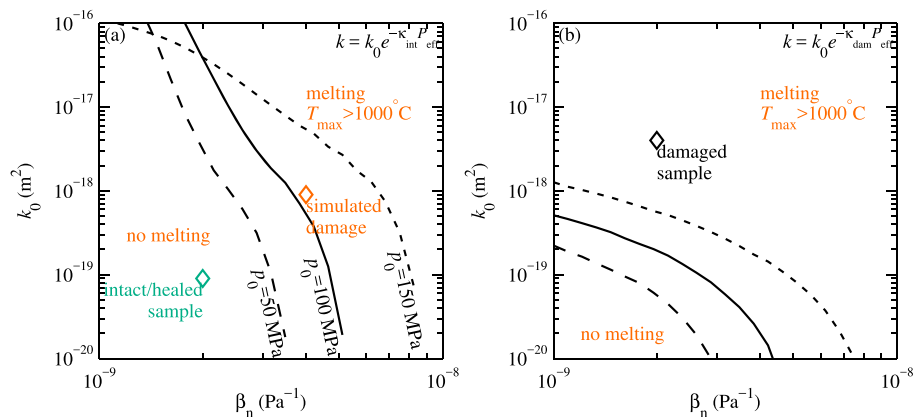

Figure 4. Contours showing the onset of melting (isotherm 1000 °C) during seismic slip using the same slip rate history as in Figure 3, as a function of nominal permeability k_0 and pore space compressibility β_n. The left and right panels are for simulations using the pressure sensitivity κ of the intact (a) and damaged tonalite (b), respectively. Solid lines correspond to an initial hydrostatic pore pressure of $p_0 = 100$ MPa, dashed lines correspond to a lower initial pore pressure of $p_0 = 50$ MPa, simulating initial dilatancy, and dotted lines correspond to $p_0 = 150$ MPa, simulating supra-hydrostatic pore pressure conditions. In panel (a), the orange symbol labeled *simulated damage* corresponds to parameter values where β_n was doubled and k_0 was increased by a factor of 10 compared to the intact values.

to reduce the increase in β_n required to observe bulk melting to only a factor of 1.5. Conversely, an initially higher pore pressure level (dotted line) tends to limit the peak temperature achieved, and a larger increase in β_n, by at least a factor of 4, would be required for melting to occur.

Figure 4b shows the results obtained from varying k_0 and β_n but using the pressure sensitivity coefficient of permeability κ_{dam} of the damaged rock (which we recall is smaller than that of the intact rock). Compared to the case with κ_{int}, changing k_0 has a stronger effect on the peak temperature, but around 1 order magnitude change is still required to significantly affect the onset of melting, while only a modest change in β_n produces dramatic variations in peak temperature, resulting in a strong control on the onset of melting.

4. Discussion and Conclusions

Our results constitute the first attempt to assess theoretical predictions of thermal pressurization, using pseudotachylytes as a natural thermometer. Despite a rather conservative choice of parameters, the predictions of peak temperature based on laboratory-derived properties of the host rock (intact or damaged-healed) are inconsistent with the presence of pseudotachylytes. Instead, using the properties of damaged, unhealed rocks found further away from the fault leads to more consistent predictions of early bulk melting.

In order to reconcile the field observations with the model prediction, one needs to increase the pore compressibility of the host rock (intact or damaged-healed) by a factor of 2 to 4. Equivalently, doubling the pore space compressibility and increasing the permeability by 1 order of magnitude will also allow reconciliation of the temperature predictions with the presence of frictional melt. These ad hoc modifications of rock properties to simulate damage were originally used by Rice (2006), and our results appear to validate this approach.

Here we assumed that free fluids were present prior to seismic slip. This assumption may not be satisfied, in which case the presence of pseudotachylytes would be a natural consequence of frictional heating. However, what our results demonstrate is that the presence of pseudotachylytes is not incompatible with the occurrence of thermal pressurization, once the effect of damage (either in terms of permeability, compressibility, or dilatancy variations) have been accounted for. Dynamic fault weakening would then proceed by a sequence of mechanisms, from an initial stage where flash heating could be the main weakening process, followed by thermal pressurization, and finally frictional melting.

The common practice when applying the principle of thermal pressurization to produce strength or temperature predictions is to use laboratory-derived rock properties on exhumed materials, neglecting dilatancy, and assuming an ambient hydrostatic pore pressure (e.g., Noda & Shimamoto, 2005; Rice, 2006; Wibberley & Shimamoto, 2005). What we show here is that all these assumptions need to be used with great caution, notably because in situ rock properties and initial pore pressure conditions are likely strongly modified by the earthquake process itself (see also Griffith et al., 2012) or by exhumation processes (e.g., cooling microfractures, although these can be easily closed by confining pressure). We also did not account for the additional sources of fluids associated with devolatilization of hydrous phases due to frictional heating: Such reactions tend to buffer fault core temperature even more efficiently than thermal pressurization (Brantut et al., 2010, 2011; Sulem & Famin, 2009) so that our modeled temperatures should be viewed as upper bounds, reinforcing the conclusion that rock properties and initial conditions must have been significantly affected by fracturing processes.

The dominant parameter controlling the efficiency of thermal pressurization is clearly the pore space compressibility, β_n, and is also the most difficult to constrain experimentally. Another key factor is the permeability; however, while permeability only influences the hydraulic diffusivity of the rock, the pore space compressibility enters in both the hydraulic diffusivity and the thermal pressurization coefficient. An increase in β_n has two competing effects: (1) It tends to reduce the hydraulic diffusivity, which would promote undrained pressurization and reduce frictional heating and (2) reduces the thermal pressurization coefficient, therefore decreasing the efficiency of the thermal pressurization mechanism. It appears that the latter effect largely dominates, and therefore even small changes in β_n, for instance, due to microcrack damage, have a large influence on the effect of thermal pressurization.

In addition, the overall low average hydraulic diffusivity, of the order of 10^{-6} m^2/s, and the short duration of seismic events, of the order of a few seconds, implies that only the first few millimeters of rock around the

slipping zone are controlling the overall behavior due to thermal pressurization. Hence, very local variations in damage have large-scale consequences on the dynamic rheology of the fault.

A striking consequence is that relatively minor variations in microcrack damage can act as a toggle switch for the onset of bulk frictional melting. In the geological record, this effect is illustrated by the patchiness and sometimes erratic occurrence of pseudotachylytes along the length of a single fault strand (Smith et al., 2013). Indeed, along the GLFZ, Griffith et al. (2012) showed that the amount of microscale damage varies significantly along strike, together with the occurrence of pseudotachylytes. Such variations are expected to have first-order consequences on the rheology of the fault and therefore on the dynamics of ruptures: Indeed, the onset of melting is typically associated with a transient strengthening (e.g., Hirose & Shimamoto, 2005) and could promote pulse-like ruptures.

The fault rocks investigated here have been extracted from a relatively immature fault, in a crystalline basement, with overall small cumulative offsets (Di Toro et al., 2004; Smith et al., 2013). The nature and impact of microcrack damage in such rocks is likely to be quite different to that in mature faults containing finely comminuted, sometimes clay-rich fault cores. The absence of reported pseudotachylytes along these mature faults might be an indicator that either mature fault rocks are less prone to damage (being already formed by comminution processes) or that damage has a relatively minor impact on the temperature achieved during seismic slip.

One key aspect of damaged fault rocks is the degree of healing or sealing of the microcracks. The geological record along the Gole Larghe Fault shows that even healed or sealed fault rocks are hosts to pseudotachylytes, and our simulation results confirm that at least some damage (in the form of an increased compressibility and permeability) must have occurred transiently to allow bulk frictional melting. Therefore, it appears that long-term damage recovery (due to healing or sealing) may be rapidly overprinted by newly generated damage during an earthquake. This implies that recovery processes may only impact the early stages of seismic slip, the later stages being largely dominated by the transient effects of newly generated damage.

References

Acosta, M., Passelègue, F. X., Schubnel, A., & Violay, M. (2018). Dynamic weakening during earthquakes controlled by fluid thermodynamics. *Nature Communications*, *9*, 3074. https://doi.org/10.1038/s41467-018-05603-9

Bernabé, Y., Mok, U., & Evans, B. (2006). A note on the oscillating flow method for measuring rock permeability. *International Journal of Rock Mechanics and Mining Sciences*, *43*(2), 311–316.

Brantut, N., Han, R., Shimamoto, T., Findling, N., & Schubnel, A. (2011). Fast slip with inhibited temperature rise due to mineral dehydration: Evidence from experiments on gypsum. *Geology*, *39*(1), 59–62.

Brantut, N., Passelègue, F. X., Deldicque, D., Rouzaud, J.-N., & Schubnel, A. (2016). Dynamic weakening and amorphization in serpentinite during laboratory earthquakes. *Geology*, *44*(8), 607–610. https://doi.org/10.1130/G37932.1

Brantut, N., & Platt, J. D. (2017). Dynamic weakening and the depth dependence of earthquake faulting. In M. Y. Thomas, T. M. Mitchell, & H. S. Bhat (Eds.), *Fault zone dynamic processes: Evolution of fault properties during seismic rupture, Geophysical Monograph Series* (Vol. 227, pp. 171–194). Washington, DC: American Geophysical Union.

Brantut, N., Schubnel, A., Corvisier, J., & Sarout, J. (2010). Thermochemical pressurization of faults during coseismic slip. *Journal of Geophysical Research*, *115*, B05314. https://doi.org/10.1029/2009JB006533

Del Moro, A., Ferrara, G., Tonarini, S., & Callegari, E. (1983). Rb-Sr systematics on rocks from the Adamello granitoids, southern Alps. *Memorie della Societa Geologica Italiana*, *26*, 285–299.

Di Toro, G., Goldsby, D., & Tullis, T. E. (2004). Friction falls towards zero in quartz rock as slip velocity approaches seismic rates. *Nature*, *427*, 436–439.

Di Toro, G., Han, R., Hirose, T., De Paola, N., Nielsen, S., Mizoguchi, K., et al. (2011). Fault lubrication during earthquakes. *Nature*, *471*, 494–498.

Di Toro, G., Pennacchioni, G., & Teza, G. (2005). Can pseudotachylytes be used to infer earthquake source parameters? An example of limitations in the study of exhumed faults. *Tectonophysics*, *402*, 3–20.

Duda, M., & Renner, J. (2013). The weakening effect of water on the brittle failure strength of sandstone. *Geophysical Journal International*, *192*, 1091–1108.

Fischer, G. J., & Paterson, M. S. (1992). Measurement of permeability and storage capacity in rocks during deformation at high temperature and pressure. In B. Evans & T. F. Wong (Eds.), *Fault Mechanics and Transport Properties of Rocks, International Geophysics Series* (pp. 187–211). London: Academic Press.

Griffith, W. A., Mitchell, T. M., Renner, J., & Di Toro, G. (2012). Coseismic damage and softening of fault rocks at seismogenic conditions. *Earth and Planetary Science Letters*, *353-354*, 219–230.

Hayward, K. S., Cox, S. F., Fitz Gerald, J. D, Slagmolen, B. J. J., Shaddock, D. A., Forsyth, P. W. F., et al. (2016). Mechanical amorphization, flash heating, and frictional melting: Dramatic changes to fault surfaces during the first millisecond of earthquake slip. *Geology*, *44*, 1043–1046. https://doi.org/10.1130/G38242.1

Hirose, T., & Shimamoto, T. (2005). Growth of molten zone as a mechanism of slip weakening of simulated faults in gabbro during frictional melting. *Journal of Geophysical Research*, *110*, B05202. https://doi.org/10.1029/2004JB003207

Jaeger, J. C., Cook, N. G. W., & Zimmerman, R. W (2007). *Fundamentals of Rock Mechanics* (4th ed.). Oxford, UK: Blackwell Publishing.

Junglas, P. (2009). WATER95 – A MATLAB® implementation of the IAPWS-95 standard for use in thermodynamics lectures. *International Journal of Engineering Education*, *25*(1), 3–18.

Lachenbruch, A. H. (1980). Frictional heating, fluid pressure, and the resistance to fault motion. *Journal of Geophysical Research*, *85*, 6097–6122.

Mase, C. W., & Smith, L. (1985). Pore-fluid pressures and frictional heating on a fault surface. *Pure and Applied Geophysics*, *122*, 583–607.

Mitchell, T. M., & Faulkner, D. R. (2012). Towards quantifying the matrix permeability of fault damage zones in low porosity rocks. *Earth and Planetary Science Letters*, *339-340*, 24–31.

Mittempergher, S., Dallai, L., Pennacchioni, G., Renard, F., & Di Toro, G. (2014). Origin of hydrous fluids at seismogenic depth: Constraints from natural and experimental fault rocks. *Earth and Planetary Science Letters*, *385*, 97–109.

Noda, H., Dunham, E. M., & Rice, J. R. (2009). Earthquake ruptures with thermal weakening and the operation of major faults at low overall stress levels. *Journal of Geophysical Research*, *114*, B07302. https://doi.org/10.1029/2008JB006143

Noda, H., & Shimamoto, T. (2005). Thermal pressurization and slip-weakening distance of a fault: An example of Hanaore fault, southwest Japan. *Bulletin of the Seismological Society of America*, *95*(4), 1224–1233.

Pennacchioni, G., Di Toro, G., Brack, P., Menegon, L., & Villa, I. M. (2006). Brittle–ductile–brittle deformation during cooling of tonalite (Adamello, southern Italian Alps). *Tectonophysics*, *427*, 171–197.

Platt, J. D., Rudnicki, J. W., & Rice, J. R. (2014). Stability and localization of rapid shear in fluid-saturated fault gouge, 2. Localized zone width and strength evolution. *Journal of Geophysical Research*, *119*, 4334–4359. https://doi.org/10.1002/2013JB010711

Rempel, A., & Rice, J. R. (2006). Thermal pressurization and onset of melting in fault zones. *Journal of Geophysical Research*, *111*, B09314. https://doi.org/10.1029/2005JB004006

Rice, J. R. (2006). Heating and weakening of faults during earthquake slip. *Journal of Geophysical Research*, *111*, B05311. https://doi.org/10.1029/2005JB004006

Rice, J. R., Rudnicki, J. W., & Platt, J. D. (2014). Stability and localization of rapid shear in fluid-saturated fault gouge, 1. Linearized stability analysis. *Journal of Geophysical Research*, *119*, 4311–4333. https://doi.org/10.1002/2013JB01071

Sibson, R. H. (1975). Generation of pseudotachylyte by ancient seismic faulting. *Geophysical Journal International*, *43*(3), 775–794. https://doi.org/10.1111/j.1365-246x.1975.tb06195.x

Smith, S. A. F., Bistacchi, A., Mitchell, T. M., Mittempergher, S., & Di Toro, G. (2013). The structure of an exhumed intraplate seismogenic fault in crystalline basement. *Tectonophysics*, *599*, 29–44.

Stipp, M., Fügenschuh, B., Gromet, L. P., Stünitz, H., & Schmid, S. M. (2004). Contemporaneous plutonism and strike-slip faulting: A case study form the Tonale fault zone north of the Adamello pluton (Italian Alps). *Tectonics*, *23*, TC3004. https://doi.org/10.1029/2003TC001515

Sulem, J., & Famin, V. (2009). Thermal decomposition of carbonates in fault zones: Slip-weakening and temperature-limiting effects. *Journal of Geophysical Research*, *114*, B03309. https://doi.org/10.1029/2008JB005912

Tinti, E., Spudich, P., & Cocco, M. (2005). Earthquake fracture energy inferred from kinematic rupture models on extended faults. *Journal of Geophysical Research*, *110*, B12303. https://doi.org/10.1029/2005JB003644

Wibberley, C. A. J., & Shimamoto, T. (2003). Internal structure and permeability of major-lip fault zones: The Median Tectonic Line in Mie Prefecture, southwest Japan. *Journal of Structural Geology*, *25*, 59–78.

Wibberley, C. A. J., & Shimamoto, T. (2005). Earthquake slip weakening and asperities explained by thermal pressurization. *Nature*, *436*(4), 689–692.